

# The Photoinduced Activity of Ni-TiO<sub>2</sub>/TiO<sub>2</sub> Multilayer Nanocomposites Synthesized by Pulse Electrodeposition Technique

S. Mohajeri\*, A. Dolati\*, M. Ghorbani

Department of Materials Science and Engineering, Sharif University of Technology, P.O.BOX 11155-9466, Tehran, I.R.Iran

\*E-mail: [smohajeri@alum.sharif.edu](mailto:smohajeri@alum.sharif.edu), [dolati@sharif.edu](mailto:dolati@sharif.edu)

Received: 26 February 2017 / Accepted: 14 April 2017 / Published: 12 May 2017

---

The sol-enhanced pulse plating (PP) technique was utilized to deposit the Ni-TiO<sub>2</sub>/TiO<sub>2</sub> multilayers on copper substrates from a Watts bath containing a TiO<sub>2</sub> sol, and the obtained coatings were heat treated at various temperatures. The characteristics of coatings were examined using scanning electron microscopy (SEM), X-ray diffraction (XRD), atomic force microscopy (AFM), X-ray photoelectron spectroscopy (XPS), and UV-visible spectrophotometry. In order to estimate the wettability of these nanostructured multilayers after exposure to UV light, the contact angle of water droplets were measured, and the photocatalytic (PC) efficiency of the multilayers were analyzed by the degradation of methyl orange (MO). The photoelectrocatalytic (PEC) activity of multilayer coatings for the decomposition of phenol was determined, and various potentials were applied to optimize the degradation efficiency under UV illumination. It was found that the multilayer heated at 450°C not only exhibited the greatest light-induced hydrophilicity, but also possessed the highest PC activity. This was justified on the basis of the highest percentage of the anatase phase present in the coating heated at 450°C, along with the maximum amount of absorbed hydroxyl groups as well as considerable roughness. The PEC efficiency of this multilayer was 97.22% for the degradation of phenol under the anodic potential of 600 mV along with 2h of simultaneous UV illumination.

---

**Keywords:** Pulse-plating, Ni-TiO<sub>2</sub>/TiO<sub>2</sub> multilayers, Photoinduced hydrophilicity, Photoelectrocatalytic degradation

## 1. INTRODUCTION

Ni matrix composites reinforced by TiO<sub>2</sub> nanoparticles have been considered as one of the most promising nanocomposites since they exhibit improved microhardness, adhesiveness, wear, and corrosion resistance, as well as self-lubricating properties [1-3]. Several techniques have been applied

to fabricate protective TiO<sub>2</sub>-containing coatings, including electrodeposition, plasma thermal spray, spray pyrolysis, chemical vapor deposition (CVD), magnetron sputtering, physical vapor deposition (PVD), and sol-gel process [4-10]. There is, however, an innovative sol-modified electrodeposition procedure that benefits from the advantages of the sol-gel process and conventional electrodeposition. Since the potential, as well as sol concentration control the deposition rate and the composition of the deposited film, the control of the codeposition process in this novel method is very high [11,12]. While for the deposition of coatings by direct current (DC) additives should be necessarily used to optimize the composition, characteristics, and the flow of electric charge, pulse plating (PP) and pulse reverse plating (PRP) procedures enable the precise selection of pertinent variables to effectively modify the microstructural features and contribute to higher percentages of embedded particles [13]. A combination of PP technique and sol-gel method can be applied to produce multilayer assemblies containing Ni-TiO<sub>2</sub> nanocomposite layers and TiO<sub>2</sub> rich layers. These nanostructures possess higher corrosion resistance and improved mechanical characteristics in comparison to pure nickel coatings as well as Ni-TiO<sub>2</sub> single layers prepared by DC, PP, and PRP [14].

Nowadays TiO<sub>2</sub>-based nanocomposite coatings have attracted significant research interest due to their high photocatalytic (PC) activity, photoinduced hydrophilicity, and photoelectrocatalytic (PEC) applications [15]. However, the photoinduced properties of TiO<sub>2</sub>-containing coatings are dramatically affected by the film structure. It is commonly accepted that the crystallographic structure and size of TiO<sub>2</sub> nanoparticles have crucial impacts upon their photoinduced activity [16], and coatings that possess crystalline structures and large surface areas per unit of mass exhibit enhanced PC behavior and excellent surface wettability. Consequently, the optimization of a coating structure is critical for the effective utilization of TiO<sub>2</sub>-containing coatings [17]. It has been reported that the TiO<sub>2</sub> coatings, in the as-deposited condition, generally have a non-crystalline nature; thus, the heat treatment of deposited TiO<sub>2</sub>-containing composites promotes their crystallinity, making them suitable for applications in photocatalysis and photoinduced hydrophilicity. Nevertheless, the annealing might dramatically affect the microstructure of coatings and adversely alter their physical or chemical characteristics. Hence, the optimization of heat treatment parameters is an essential measure that should be taken to obtain the most favorable photochemical properties [18].

The excitation of TiO<sub>2</sub> nanoparticles under the UV light transfers electrons to the conduction band, and due to the extraction of electrons from the valance band, positive holes are generated. These electron-hole pairs migrate to the surface of TiO<sub>2</sub> nanoparticles and produce hydroxyl radicals that are capable of decomposing pollutants. Nevertheless, the excited electrons and holes tend to recombine promptly, deteriorating the PC behavior of TiO<sub>2</sub> nanoparticles [19]. In order to inhibit the undesirable electron-hole recombination, an external potential is applied via the PEC process to boost the capability of TiO<sub>2</sub> particles for photoconversion [20]. Although many studies have reported the increased photoactivity of TiO<sub>2</sub>-based multilayers [21, 22], very few researchers have examined the PEC efficiency of multilayer nanocomposites, and limited research has so far been reported on the photoinduced properties of multilayer systems composed of Ni matrix composites reinforced with titania nanoparticles.

In our previous work, we have synthesized multilayers containing Ni-TiO<sub>2</sub> and TiO<sub>2</sub> rich layers by pulse current and increased the amount of the codeposited TiO<sub>2</sub> nanoparticles by restricting the

nickel plating [14]. The current study examined the effects of various temperatures upon the phase structure of Ni-TiO<sub>2</sub>/TiO<sub>2</sub> multilayers, the amount of surface hydroxyl content after UV irradiation, and the photoinduced hydrophobicity and PC activity. This survey concentrates on the estimation of the optimal heat treatment temperature with respect to the obtained results from photoinduced properties (PC activity and hydrophilicity) and explores the influence of several bias potentials on the PEC efficiency of the Ni-TiO<sub>2</sub>/TiO<sub>2</sub> multilayer for the degradation of contaminants.

## 2. EXPERIMENTAL

TiO<sub>2</sub> sol was prepared by mixing titanium tetraisopropoxide (97%, Sigma-Aldrich, UK) with ethanol (96%, Merck, Germany). A mixture of deionized water and nitric acid (70%, Sigma-Aldrich, UK) was utilized to hydrolyze the sol under intensive stirring for 2h, while keeping the relative humidity constant. The obtained TiO<sub>2</sub> sol was mixed in a Watts solution consisting of NiSO<sub>4</sub>, NiCl<sub>2</sub>, H<sub>3</sub>BO<sub>3</sub>, and sodium dodecyl sulfate (SDS), after storage for 24h under a vacuum of 10 m Torr. The PP technique was applied to deposit Ni-TiO<sub>2</sub>/TiO<sub>2</sub> multilayers on copper substrates. To optimize the deposition potentials suited for the deposition of multilayers, cyclic voltammograms were recorded by an EG&G Princeton Applied Research (PAR) potentiostat. Additional details about the selection of the electrochemical factors for the fabrication of the designed multilayers were reported elsewhere [14]. Deposition times were modified to obtain deposits with the average thickness of ~15μm. Multilayer coatings were dried at 90°C for 10 minutes and subsequently heated at 100, 200, 300, 400, 450, and 550°C for 3h. These samples were mentioned as Ni-TiO<sub>2</sub>/TiO<sub>2</sub>-300, Ni-TiO<sub>2</sub>/TiO<sub>2</sub>-400, Ni-TiO<sub>2</sub>/TiO<sub>2</sub>-450, and Ni-TiO<sub>2</sub>/TiO<sub>2</sub>-550 in the text. The morphology of multilayers were examined by a scanning electron microscope (SEM) (Model TESCAN ILMU). The phase structure of Ni-TiO<sub>2</sub>/TiO<sub>2</sub> multilayer thin films were identified by a Philips PW-3040 X-ray diffractometer (XRD). A Nanoscope III AFM scanner was utilized to assess the surface morphology and average roughness of the coatings by the atomic force microscopy. The surface chemical states of multilayers were verified using the X-ray photoelectron spectroscopy (XPS, JEOL). The photoinduced wettability of multilayers was examined via estimating the variations of the water contact angle versus the duration of UV irradiation as well as heat treatment temperature. The applied ultraviolet source was a UV/vis mercury lamp with the intensity of 0.5 mW.cm<sup>-2</sup> aligned perpendicular to the surface of multilayers with an exposed area of 1×1 cm. Contact angle measurements were carried out at ambient via a CCTV camera by placing a water droplet with the volume of 4 μL on each specimen. The water contact angel for each specimen was recorded as the mean of the two repeated measurements. PC activity of the TiO<sub>2</sub>-containing multilayers was assessed by the photoinduced decomposition of the methyl orange (MO) aqueous solution. For the estimation of the PC activity, multilayers were irradiated by the UV light according to the procedure applied in the wettability tests. The concentration of the aqueous MO was determined via a JENWAY spectrophotometer by measuring the absorbance at 467 nm. PEC degradation experiments were performed in a cell containing the copper coated with the Ni-TiO<sub>2</sub>/TiO<sub>2</sub> multilayer nanocomposite (working electrode, 1×1 cm) and a platinum sheet (counter-electrode, 2×2 cm), with reference to a saturated calomel electrode (SCE). The supplied bias and current were controlled using

an Autolab PGSTAT 302 electrochemical system. The samples were irradiated by UV light under the same condition mentioned for the PC experiments, and the UV lamp was placed 10 cm away from the multilayer nanocomposite. The cell was filled with an aqueous solution of 100 mg/L phenol and 0.1 mol/L  $\text{Na}_2\text{SO}_4$  (pH=7). The bias potentials of 0, 200, 400, 600, and 800 mV vs. SCE were applied and the degradation rate of phenol was examined by measuring its absorbance at 432 nm on a Hitachi 3100 spectrophotometer.

### 3. RESULTS AND DISCUSSION

#### 3.1. Preparation of Ni-TiO<sub>2</sub>/TiO<sub>2</sub> multilayer nanostructures

The optimal pulse potentials for the fabrication of Ni-TiO<sub>2</sub>/TiO<sub>2</sub> multilayer structures were determined by plotting the cyclic voltammetry (CV) curve of the Ni-TiO<sub>2</sub> system in a mixture of the Watts solution and TiO<sub>2</sub> sol. According to Fig. 1, the simultaneous deposition of Ni ions and TiO<sub>2</sub> nanoparticles in the Ni-TiO<sub>2</sub> composite takes place at -900 mV, where the electrocrystallization process of nickel is governed by the three-dimensional instantaneous nucleation [23]. Furthermore, the cathodic peak at -700 mV is associated with the restricted deposition of Ni by the diffusion current; thus, we applied the potential of -700 mV to deposit TiO<sub>2</sub>-saturated layers in the Ni-TiO<sub>2</sub>/TiO<sub>2</sub> multilayer structure. The durations for the application of the pulse potentials of -900 and -700 mV were chosen 900 and 200 ms, respectively, with regard to the results of our earlier investigation [14] about the impacts of PP variables upon the fabrication of Ni-TiO<sub>2</sub>/TiO<sub>2</sub> multilayer structures. It was determined that as the pulse potential of -700 mV is applied for longer durations, the TiO<sub>2</sub> content is enhanced, reaching 18.47 wt.% for the duration of 200 ms. This increased TiO<sub>2</sub> content can be attributed to the extended pulse duration at -700 mV, where the Ni deposition is restricted by the diffusion control, leading to the deposition of composite layers saturated with TiO<sub>2</sub> particles.

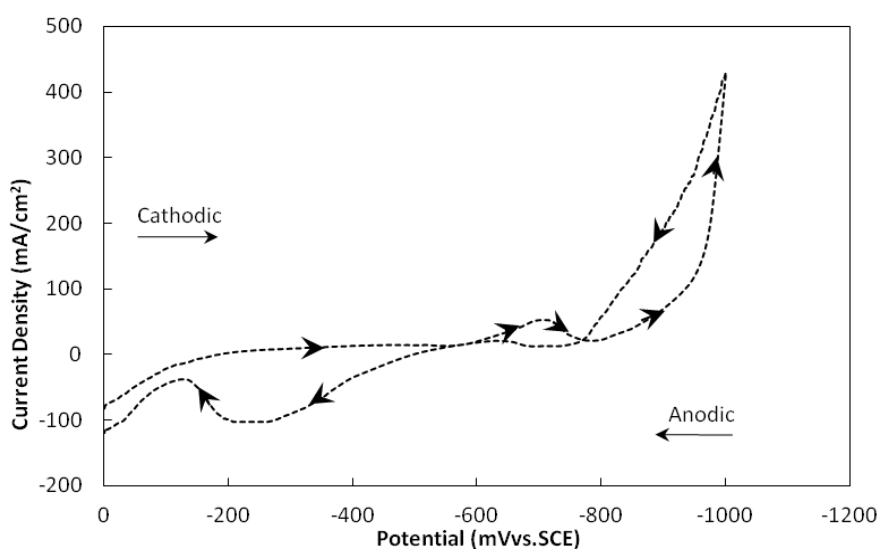


**Figure 1.** CV curve for the deposition of Ni-TiO<sub>2</sub> in a Watts solution containing the TiO<sub>2</sub> sol, scan rate=10 mV/sec.

The surface and cross-section SEM images of the Ni-TiO<sub>2</sub>/TiO<sub>2</sub> multilayer are displayed in Fig. 2. It is indicated that clusters of TiO<sub>2</sub> nanoparticles emerge as gray aggregates on the surface of the coating (Fig. 2 (a)), and a laminated structure is observed in the cross-sectional view of the thin films in which the consecutive layers of Ni-TiO<sub>2</sub> and TiO<sub>2</sub>-saturated nanocomposites with an approximate thickness of 392 nm are detected (Fig. 2 (b)).

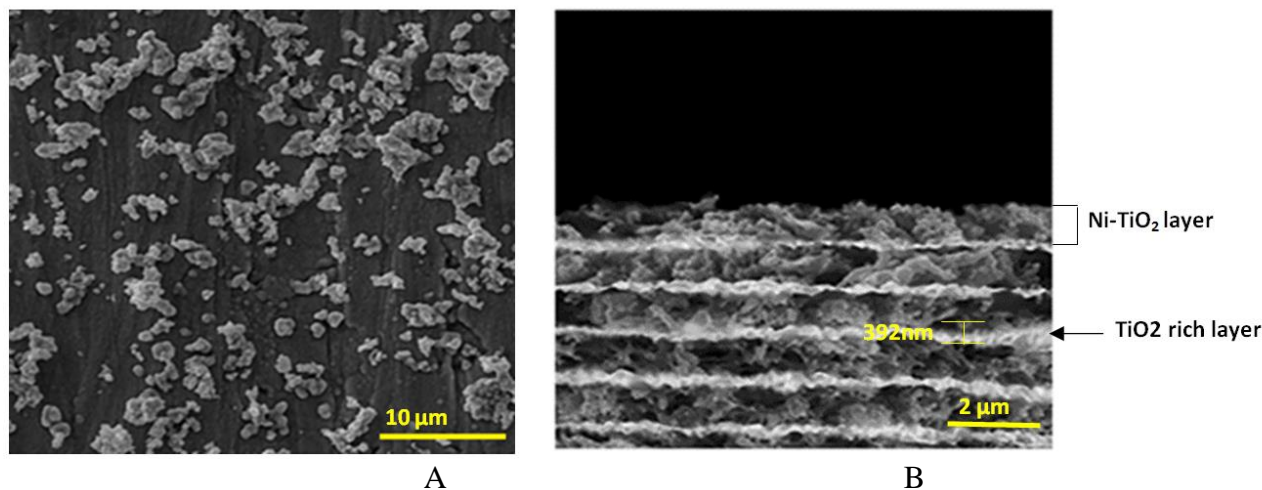


**Figure 2.** (a) Surface and (b) cross-sectional morphology of the multilayer coating deposited by the PP.

### 3.2. Crystallinity and surface roughness

The effects of thermal treatment on the phase transformation in Ni-TiO<sub>2</sub>/TiO<sub>2</sub> multilayers was explored, and the XRD spectra of TiO<sub>2</sub> particles separated from multilayer deposits after being heat treated at different temperatures (100, 200, 300, 400, 450, 550 °C) for 3h are depicted in Fig. 3. As shown, the TiO<sub>2</sub> particles of films heated at 100 and 200 °C are not completely crystallized; however, for the sample heated at 200 °C, a broad peak is observed at around  $2\theta = 25.25^\circ$ . Formation of the anatase phase begins at temperatures higher than 200 °C, and for the samples heated at 300, 400, and 450 °C, the peaks at  $2\theta = 25.25^\circ$ ,  $2\theta = 37.82^\circ$ , and  $2\theta = 48.21^\circ$  represent the (101), (004), and (200) crystal planes of anatase TiO<sub>2</sub>, respectively. All peaks coincide well with JCPDS no.1272-21. Enhanced intensity and decreased width of the diffraction peaks of anatase are observed with the increase of the temperature in the range of 300-450 °C, indicating an increased crystallinity and larger sizes of TiO<sub>2</sub> crystallites. The XRD pattern of TiO<sub>2</sub> particles separated from the multilayer heated at 550 °C reveals the anatase peaks as well as three other weak peaks at diffractive angles of  $2\theta = 27.4^\circ$ ,  $2\theta = 36.1^\circ$ , and  $2\theta = 41.2^\circ$ , signifying (110), (101), and (111) planes of the rutile, respectively. These peaks accord well with those in JCPDS no.1276-21 card for the rutile TiO<sub>2</sub>. As the rutile peaks emerge at temperatures higher than 450 °C, the anatase peaks progressively weaken while their widths decrease since the titania crystallites grow further. Although the conversion of pure anatase to rutile initiates at temperatures around 600 °C, the experimental temperatures recorded in literature for this conversion are between 400 to 1200 °C depending on the synthesis procedures, types of materials, and estimation methods [24]. Fig.

3 demonstrates that for our designed multilayers, the anatase to rutile transformation occurs at temperatures higher than 450°C.

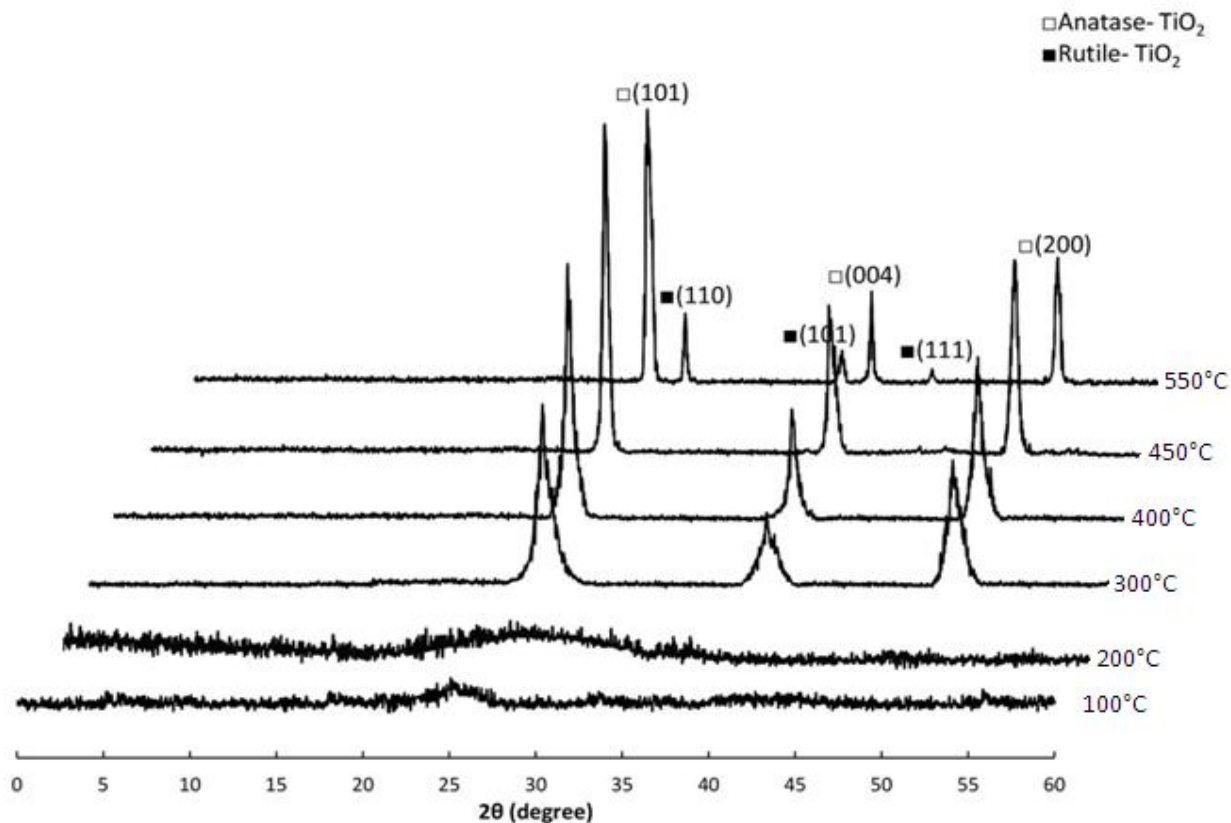


**Figure 3.** X-Ray diffraction patterns of titanium dioxide particles obtained from Ni-TiO<sub>2</sub>/TiO<sub>2</sub> multilayers after 3h of heat treatment at 100, 200, 300, 400, 450, and 550°C.

AFM analyses of the surface of multilayer nanocomposites are illustrated in Fig. 4. This figure confirms that the roughness and microstructure of the coatings are apparently influenced by heat treatment. At 100°C, the multilayer possesses the minimum roughness and exhibits a fine-grained smooth surface, for which the average size of particles are in the range of 40 to 50 nm (Fig. 4 (a)). As claimed by SEM analysis in Fig. 2, the spherical particles distributed in the multilayers are clusters of numerous TiO<sub>2</sub> nanograins. With the increase of the temperature from 200 to 450°C, the size of spherical particles increases from 60 to 90 nm, and the average distances between the highest peak and lowest valley in each sample increase as well (Fig. 4 (b) to (f)). The quantities of surface roughness were extracted from AFM data and as presented in Table 1, the average roughness (Ra) for the multilayer heated at 100°C is 67 nm.

Roughness measurements suggest that the surface roughness of the multilayers increases at higher heat treatment temperatures, reaching 203 nm for the multilayer heat treated at 550°C. The remained carbon produced in the sol-gel process is removed during heat treating at higher temperatures and this accounts for the enhanced surface roughness [25].



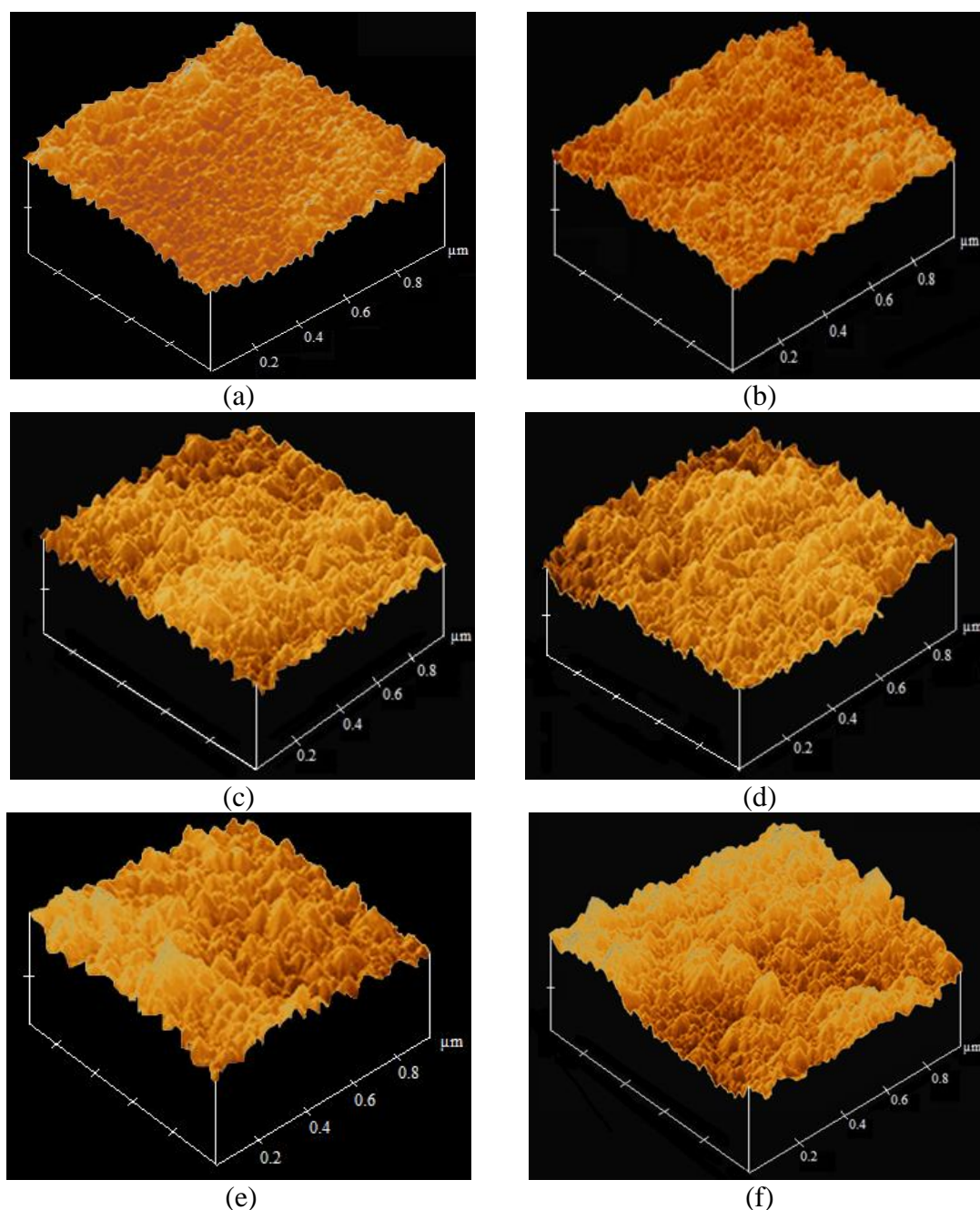


**Figure 4.** AFM images of the Ni-TiO<sub>2</sub>/TiO<sub>2</sub> multilayers after 3h of heat treatment at (a) 100, (b) 200, (c) 300, (d) 400, (e) 450, and (f) 550 °C.

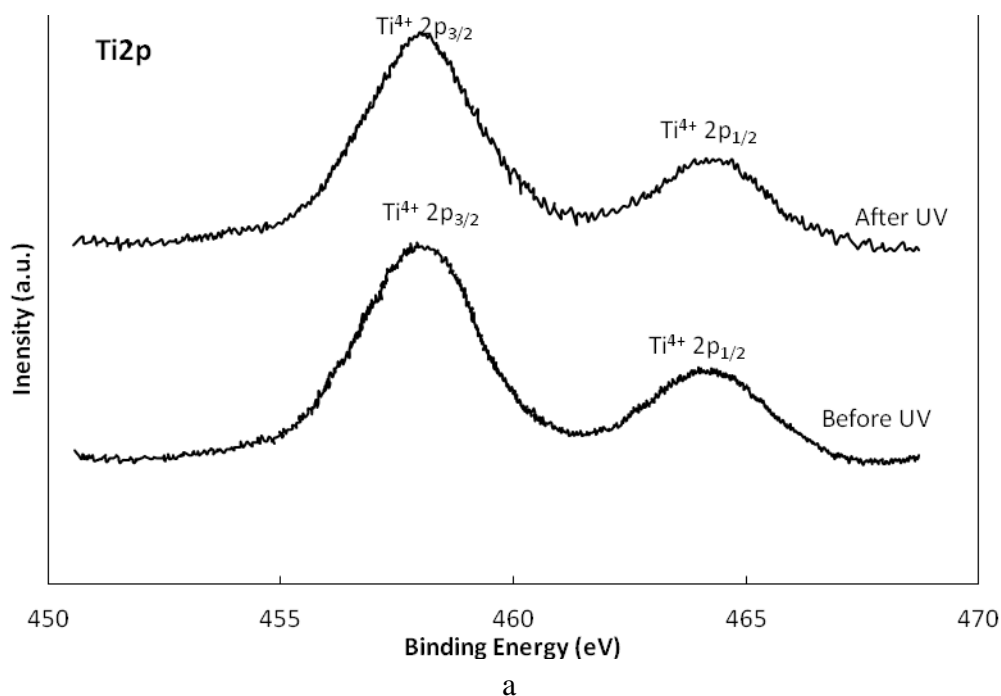
**Table 1.** Physico-chemical characteristics of the TiO<sub>2</sub> particles separated from Ni-TiO<sub>2</sub>/TiO<sub>2</sub> multilayers heat treated at 100-550 °C for 3h.

Heat treatment temperature (°C)	Phase structure	Average roughness (nm)	%OH (before UV)	%OH (after UV)
100	----	67	0.37	0.48
200	----	84	1.20	1.61
300	Anatase	113	4.15	10.39
400	Anatase	126	6.79	14.23
450	Anatase	178	9.41	20.56
550	Anatase-Rutile	203	8.52	18.02

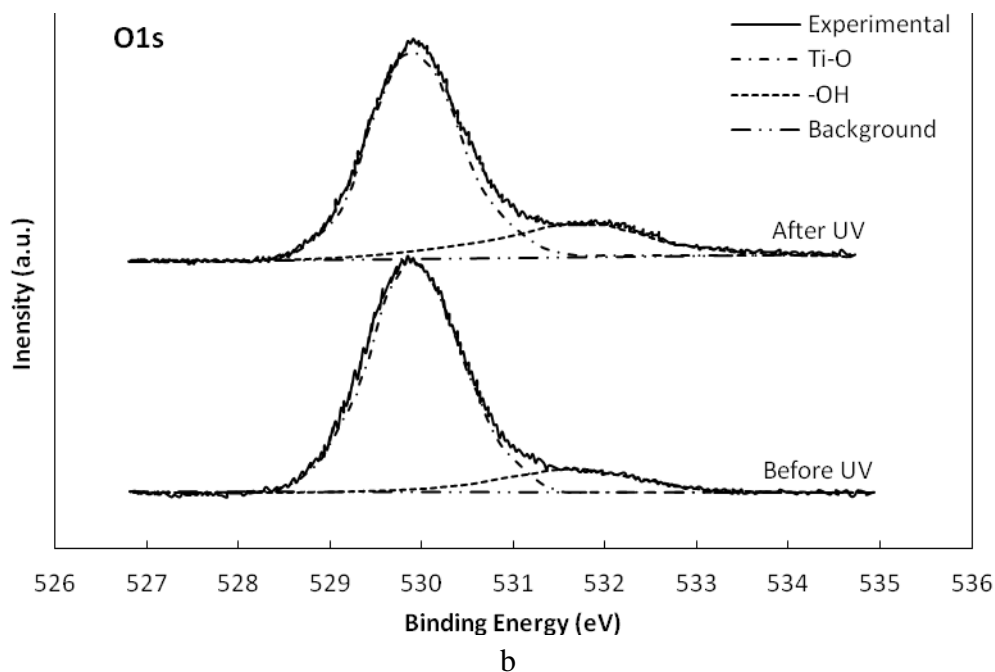
### 3.3. Surface analysis by XPS

Fig. 5 depicts the XPS spectra of Ti 2p and O 1s for the Ni-TiO<sub>2</sub>/TiO<sub>2</sub> multilayer after 3h of heat treatment at 450 °C for 3h, before and after 60 min of UV illumination. According to Fig. 5 (a), the Ti 2p peaks appear at 457.9 eV and 463.6 eV, and UV light does not alter the oxidation state of titanium from Ti<sup>4+</sup> to Ti<sup>3+</sup> in the TiO<sub>2</sub>-containing multilayer [26]. No significant changes are observed in the binding energy, intensity, and width of the peaks in the Ti 2p spectra, before and after UV illumination. With regard to literature reports, the Ti<sup>4+</sup> ion receives a photoelectron, under UV light, which can be trapped and tend to reduce Ti<sup>4+</sup> cations to Ti<sup>3+</sup> state [27]. However, for our studied multilayer, the Ti valence state does not change during 60 min of UV exposure, and the XPS does not detect the intermediate state of Ti<sup>3+</sup> ion.

As shown in the XPS spectra of oxygen in Fig. 5 (b), the 529.9 eV peak signifies the Ti-O bonding in TiO<sub>2</sub> nanoparticles, while the 531.9 eV peak displays the Ti-OH bonding (i.e., hydroxyl groups) [28]. The area under the Ti-OH peak expands after 1h of UV irradiation due to an increase in the absorption of water molecules and, consequently, the increase of surface OH group density under the UV light. The increment of OH groups on the surface of multilayers after UV irradiation can be justified by the principle of TiO<sub>2</sub> photocatalysis. It should be noted that upon the UV illumination of TiO<sub>2</sub>, electron-hole pairs are produced. The holes produced by UV irradiation tend to interact with the O<sup>2-</sup> species on the surface of TiO<sub>2</sub> nanoparticles to form O<sup>-</sup> trapped holes that impair the strength of Ti-O bond and induce the generation of oxygen vacancies. These vacancies absorb and dissociate water and generate surface hydroxyl groups. The increase in hydroxyl content can lead to the photoinduced superhydrophilicity and PC activity of the TiO<sub>2</sub>-containing multilayer [25]. The variations of surface OH concentrations on Ni-TiO<sub>2</sub>/TiO<sub>2</sub> multilayers heated at 100 to 550 °C for 3h, prior and after 1h of UV illumination, are represented in Table 1.







**Figure 5.** XPS spectra (a) Ti 2p and (b) O 1s for the Ni-TiO<sub>2</sub>/TiO<sub>2</sub> multilayer heated at 450°C, before and after 1h of UV irradiation.

The percentage of OH concentration (%) is calculated from the O1s spectra by dividing the area under the peak located at higher binding energy into the sum of the area under the both peaks. The results indicate that irradiation of UV light significantly enhance the surface OH concentration, regardless of the heat treatment temperature.

As mentioned before, the increase of OH% is due to the absorbance of water molecules on the defective sites of TiO<sub>2</sub> nanoparticles in the multilayers, and their subsequent oxidation by electron-hole pairs which lead to the production of hydrogen gas and hydroxyl radicals. Based on the results, the density of hydroxyls on the surface of the multilayer heated at 450°C is evidently higher compared to the coatings heated at 100 to 400°C. The difference in the hydroxyl content among the multilayers are attributed to their dissimilar XRD patterns. According to Fig. 3, for the multilayer heated at 450°C, the intensity of anatase peaks are maximum and a higher volume of TiO<sub>2</sub> is crystallized and thus, a greater amount of hydrophilic anatase phase is present in the coating. However, based on the data in Table 1, the density of hydroxyl groups declines notably for the coating treated at 550°C. This behavior is due to the fact that the multilayer heated at 550°C contains lower amounts of anatase crystallites which their sizes are larger and their active surface area for the formation of hydroxyl groups is lower than those of the multilayer heated at 450°C. Moreover, the formation of the less hydrophilic rutile phase at 550°C can be another reason for the detection of lower density of surface hydroxyl groups on this multilayer.

## 3.4. Photoinduced hydrophilicity

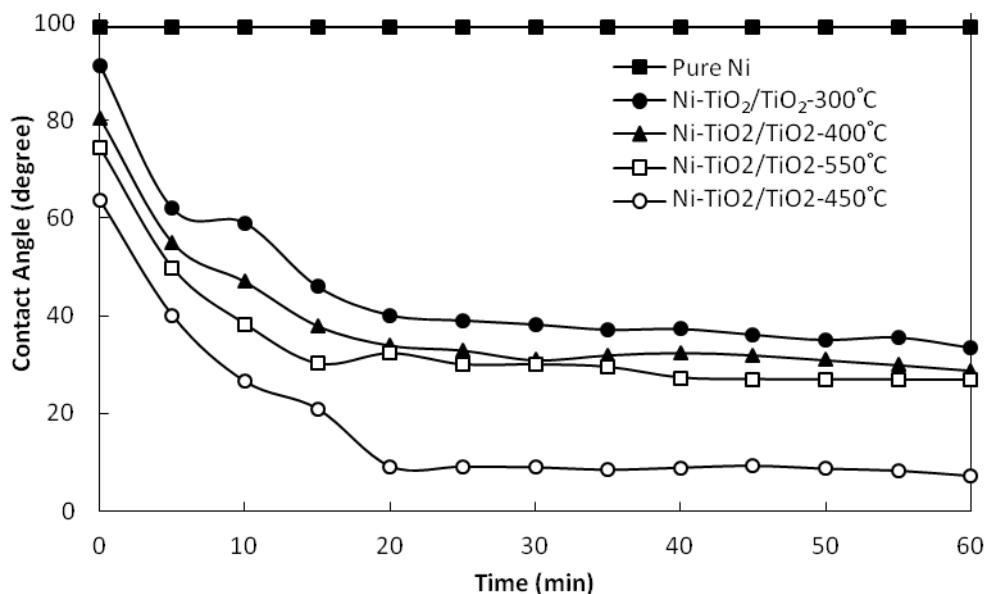


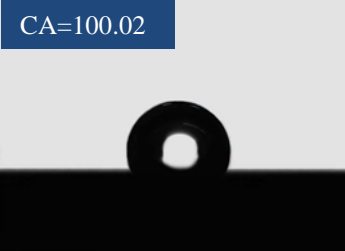
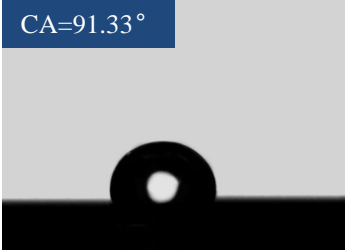
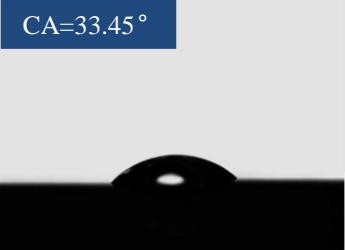
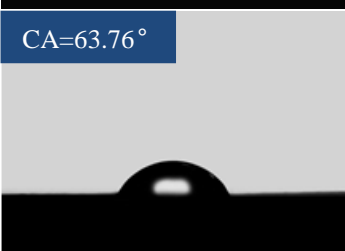
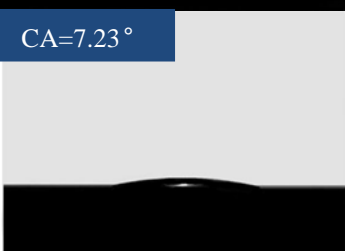
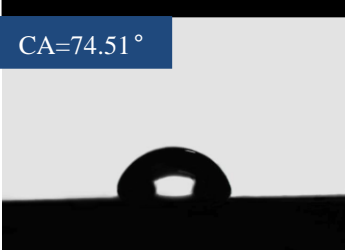
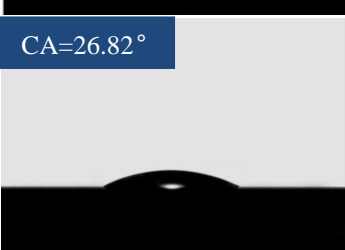
**Figure 6.** Changes of water contact angles versus the UV illumination time for the pure Ni and Ni-TiO<sub>2</sub>/TiO<sub>2</sub> multilayers heated for 3h at different temperatures.

In order to estimate the hydrophilicity of Ni-TiO<sub>2</sub>/TiO<sub>2</sub> multilayer coatings heat treated at 300 to 550°C for 3h, variations of the water contact angles were detected under the UV illumination as a function of the temperature as well as the illumination time. The pure nickel deposit was investigated for comparison. According to Fig. 3, the films heated at 100 and 200°C are not completely crystallized, so they are not expected to show a strong hydrophilic behavior, and thus, we did not include them in our water contact angle measurements. As illustrated in Fig. 6, the water contact angle of the pure Ni does not vary with the illumination time and a constant value of 99° is detected, indicating the hydrophobic feature of this coating. However, the water contact angle for multilayer coatings depends not only on the heat treatment temperature but also on the time of UV irradiation. As depicted, for the multilayers heated at various temperatures, the contact angles decrease with the increase of the illumination time, and for the structures heated at 300, 400, and 550°C, contact angles after 1h of irradiation are estimated to be approximately 33.45°, 28.87°, and 26.72°, respectively. The multilayer heated at 450°C exhibits the maximum hydrophilicity, for which the contact angle prior to UV irradiation is 63.76° and after 1h of UV irradiation this value reduces to 7.23°.

Images of water droplets on the pure Ni and Ni-TiO<sub>2</sub>/TiO<sub>2</sub> multilayers are represented in Table 2. Before UV irradiation, the value of contact angles for the multilayer structures heated at higher temperatures are lower, and after UV irradiation for 1h, a similar trend is observed. This could be ascribed to the surface roughness that dramatically affects the surface hydrophilicity. As shown in Table 1 and Fig. 4, increased heat treatment temperatures enhance the roughness of the coatings. The Wenzel equation [29] suggests that hydrophilic surfaces with higher roughness values exhibit lower water contact angles and further increase the degree of the surface hydrophilicity. Moreover, the surface chemistry and particularly higher densities of hydroxyl groups are considered as the principal

parameters that have significant impacts on the hydrophilicity of Ni-TiO<sub>2</sub>/TiO<sub>2</sub> multilayer films heat treated at higher temperatures.

**Table. 2.** The shape of water drops on the surface of the pure Ni and multilayer coatings heat treated at different temperatures, before and after 1h of UV irradiation.

Coating- temperature (°C)	Before UV irradiation	After 1h of UV irradiation
Pure Ni-not heated	 CA=100.02	 CA=100.02
Ni-TiO <sub>2</sub> /TiO <sub>2</sub> -300	 CA=91.33°	 CA=33.45°
Ni-TiO <sub>2</sub> /TiO <sub>2</sub> -400	 CA=80.42°	 CA=28.87°
Ni-TiO <sub>2</sub> /TiO <sub>2</sub> -450	 CA=63.76°	 CA=7.23°
Ni-TiO <sub>2</sub> /TiO <sub>2</sub> -550	 CA=74.51°	 CA=26.82°

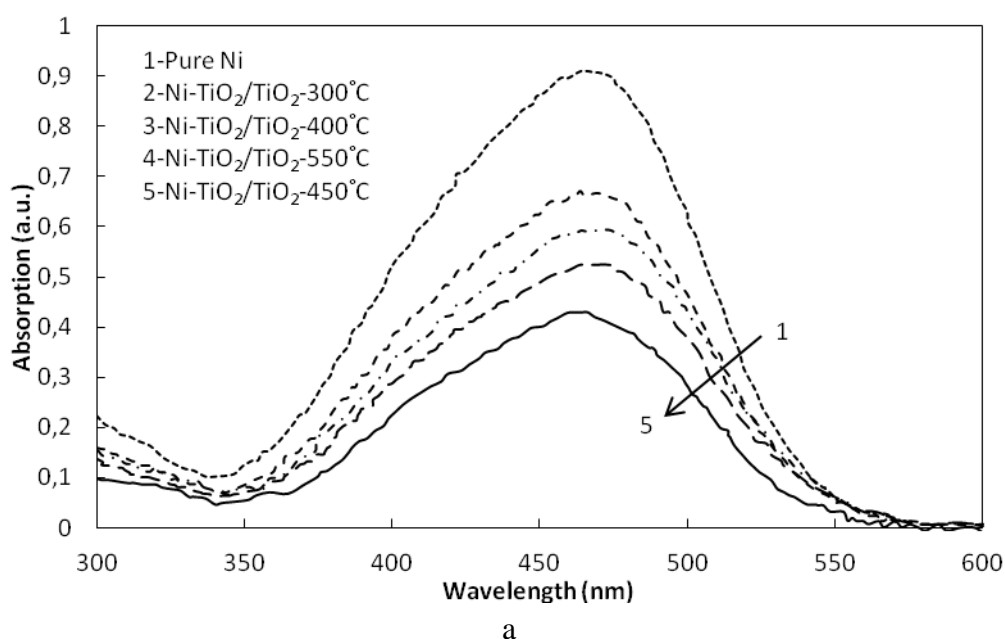
However, the composite multilayer deposit heated at 450°C reveals the minimum water contact angel and therefore the optimum photoinduced hydrophilicity, as compared to the coating heated at 550°C. The lower content of surface hydroxyl groups (as presented in Table 1), the growth of anatase

crystallites which is indicative of a reduced active area, and the conversion of the hydrophilic anatase to less hydrophilic rutile (as depicted in Fig.3) are suggested to be responsible for the larger contact angle and lower hydrophilicity of  $\text{TiO}_2$ -containing multilayer heated at  $550^\circ\text{C}$  in comparison to the coating heated at  $450^\circ\text{C}$ .

### 3.5. Photocatalytic activity

To evaluate the influence of the heat treatment temperature upon the PC efficiency of Ni- $\text{TiO}_2/\text{TiO}_2$  multilayer samples and the pure nickel coating, photoinduced decomposition tests of 10 mg/L MO solutions were implemented under the UV irradiation. Fig. 7 (a) demonstrates the UV spectra of aqueous MO over the wavelengths of 300-600 nm during the photodegradation, after 5h of UV irradiation on the pure Ni and Ni- $\text{TiO}_2/\text{TiO}_2$  multilayers. From the spectra, it can be seen that as compared with the absorbance of UV in the MO degraded with pure Ni, the absorbance of UV in the MO degraded with  $\text{TiO}_2$ -containing multilayers is lower due to the decomposition of higher volumes of MO by the multilayers which can consequently accelerate the transmittance of UV light through the MO solution. The amount of UV light that is absorbed by the MO decomposed by multilayers decreases as the heat treatment temperature is increased, and the maximum absorbance for the coating heated at  $450^\circ\text{C}$  reaches 0.42 nm, confirming that this multilayer coating has an outstanding PC performance.

The curves of the PC decomposition of MO by the pure Ni as well as Ni- $\text{TiO}_2/\text{TiO}_2$  multilayer coatings after heat treatment at different temperatures during 5h of UV irradiation are displayed in Fig. 7 (b). Predictably, the pure nickel deposit has almost no effect on the decomposition of MO and does not exhibit a detectable PC behavior, confirming the results obtained by other researchers [30]. Conversely, multilayer coatings exhibit considerable PC characteristics, and their PC activity increases with an increase in the irradiation time.



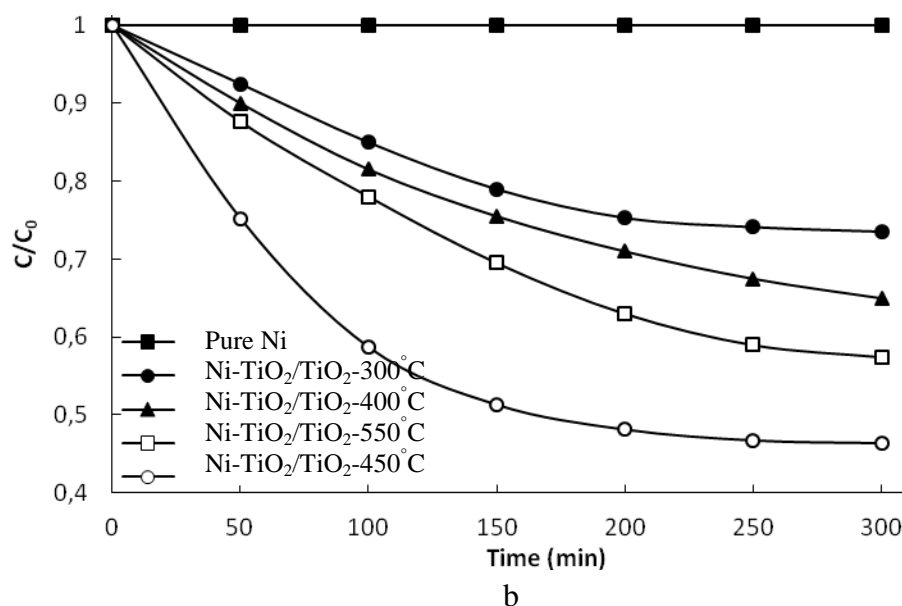


**Figure 7.** (a) UV-vis spectra for MO after the photodegradation tests by the pure nickel and multilayer coatings and (b) photodegradation extent of MO as an organic pollutant by nanocomposite multilayers heat treated at different temperatures, under UV illumination.

According to the “site proximity” model [31], the enhancement of the PC activity of Ni-TiO<sub>2</sub>/TiO<sub>2</sub> multilayer composites is due to the adsorption function of Ni matrix and the presence of TiO<sub>2</sub> nanoparticles that serve as photoconversion sites for the decomposition of pollutant molecules at the interface. Moreover, the results indicate that for all the multilayers with an equal TiO<sub>2</sub> content (18.47 wt.%), heat treatment temperatures can favor the PC efficiency.

The multilayer heated at 550°C exhibit superior PC activity compared to the films heated at 300 and 400°C, due to its enhanced surface roughness (see Table 1) and the consequent increase in the number of active sites that interact with the contaminant molecules. This in turn facilitates the formation of hydroxyl and superoxide radicals (OH<sup>•</sup>, H<sub>2</sub>O<sub>2</sub>, O<sub>2</sub><sup>•</sup>, etc.) responsible for attacking the pollutant molecules and thereby increases the pollutant removal efficiency [32]. Based on the XRD data in Fig. 3, the minor reduction in the PC activity of the multilayer at 550°C compared to that of 450°C might be due to the phase transformation of the embedded TiO<sub>2</sub>, as heating at 550°C expedites the conversion of anatase to rutile, and subsequently leads to the grain growth of TiO<sub>2</sub> particles. The higher amounts of anatase TiO<sub>2</sub> nanoparticles in the multilayers accelerate the degradation of the contaminant. Thus, the optimum PC activity was detected for the multilayer heated at 450°C with the best crystallinity of anatase compared to the other multilayers, for which a 53.64% pollutant degradation was achieved after 5h of UV illumination.

Fig.8 illustrates the optical photos of samples investigated by the PC experiment after 5h of UV illumination. This figure confirms that the pure nickel cannot effectively contribute to the degradation of MO, while multilayers can efficiently catalyze the photodegradation. MO molecules are almost degraded by the multilayer heated at 450°C and the solution becomes pale yellow, indicating that this multilayer has a great PC ability. It is noteworthy to mention that the PC performance of the multilayer

nanostructures accompanied by their simultaneous hydrophilic behavior impart self-cleaning properties to the surfaces and make them very useful for industrial and commercial systems.

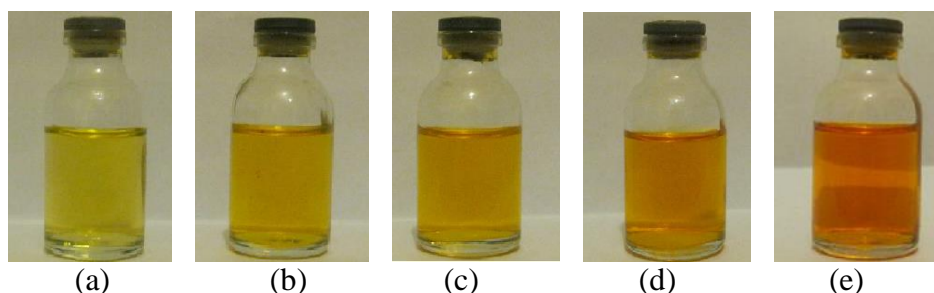


**Figure 8.** Optical photos of PC experiments by (a) pure Ni, and multilayers heated at (b) 300, (c) 400, (d) 450, and (e) 550 °C after 300 min of UV illumination.

### 3.6. Photoelectrocatalytic activity

As mentioned earlier, the Ni-TiO<sub>2</sub>/TiO<sub>2</sub> multilayer heated at 450 °C provides the maximum efficiency for the PC degradation of contaminants, and herein, the flat band potential ( $E_{fb}$ ) of the TiO<sub>2</sub> nanoparticles in this multilayer is measured using the photocurrent onset potential ( $E_{on}$ ). Fig. 9 (a) indicates the photocurrent-potential curves obtained for the Ni-TiO<sub>2</sub>/TiO<sub>2</sub> multilayer-coated electrode after heat treatment at 450 °C, in a 0.1 M Na<sub>2</sub>SO<sub>4</sub> solution (pH=7) with and without UV irradiation by scanning the potential between -800 and +800 mV vs. SCE at 10 mV/s scan rate. By comparing curves 1 and 2, it is evident that the dark current produced by the TiO<sub>2</sub> nanoparticles is negligible and the electrode coated by the multilayer does not exhibit a PEC behavior. However, under UV illumination with the light at  $\lambda > 320$  nm, the anodic current increases over the entire applied potential range, and the multilayer coated electrode reveals obviously enhanced anodic photocurrent response. Such behavior is due to the instant separation of the photoactivated electrons and holes within TiO<sub>2</sub> particles in the film, as well as the subsequent transport of more electrons in the circuit that enhance the PEC activity of the multilayer-coated anode.

Based on the photocurrent theory, during the exposure of TiO<sub>2</sub>-containing multilayers to the bulk solution interface, the surface band bows and generates an electrical field. Consequently, the photoinduced electrons transfer in the electric field and produce a photocurrent. Application of a reverse potential can partially compensate for the electric field, and the applied potential for which the current reaches zero is specified as the flat band potential. Generally, the discrepancy between the  $E_{fb}$  and the conduction band potential ( $E_{cb}$ ) is disregarded, and these two quantities are estimated as equal values [33]. Although the potential at zero current is frequently defined as the  $E_{fb}$ , this estimation is not accurate due to the plausible electron-hole recombination. According to Butler's method [34], the plot of photocurrent against potential is applied to calculate  $E_{fb}$ , through the following formula:

$$J_{ph}^2 = (2 q \epsilon \epsilon_0 \Phi_0^2 \alpha^2 / N_d) (E - E_{fb}) \quad (1)$$

Where the photocurrent density,  $J_{ph}$ , is expressed as a function of the elementary charge,  $q$ , the relative dielectric constant,  $\epsilon$ , the permittivity of vacuum,  $\epsilon_0$ , the photon flux,  $\Phi_0$ , the absorption

coefficient,  $\alpha$ , the donor concentration in the semiconductor,  $N_d$ , the electrode potential,  $E$ , and the flat band potential,  $E_{fb}$ . As depicted in Fig. 9 (b), the plot of  $J_{ph}^2$  against potential crosses the horizontal axis at  $E_{fb}$ . From this graph, the flat band potential value of around -672 mV vs. SCE is obtained for the  $TiO_2$ -containing multilayer which is consistent with the values observed by other researchers for the anatase phase [35].

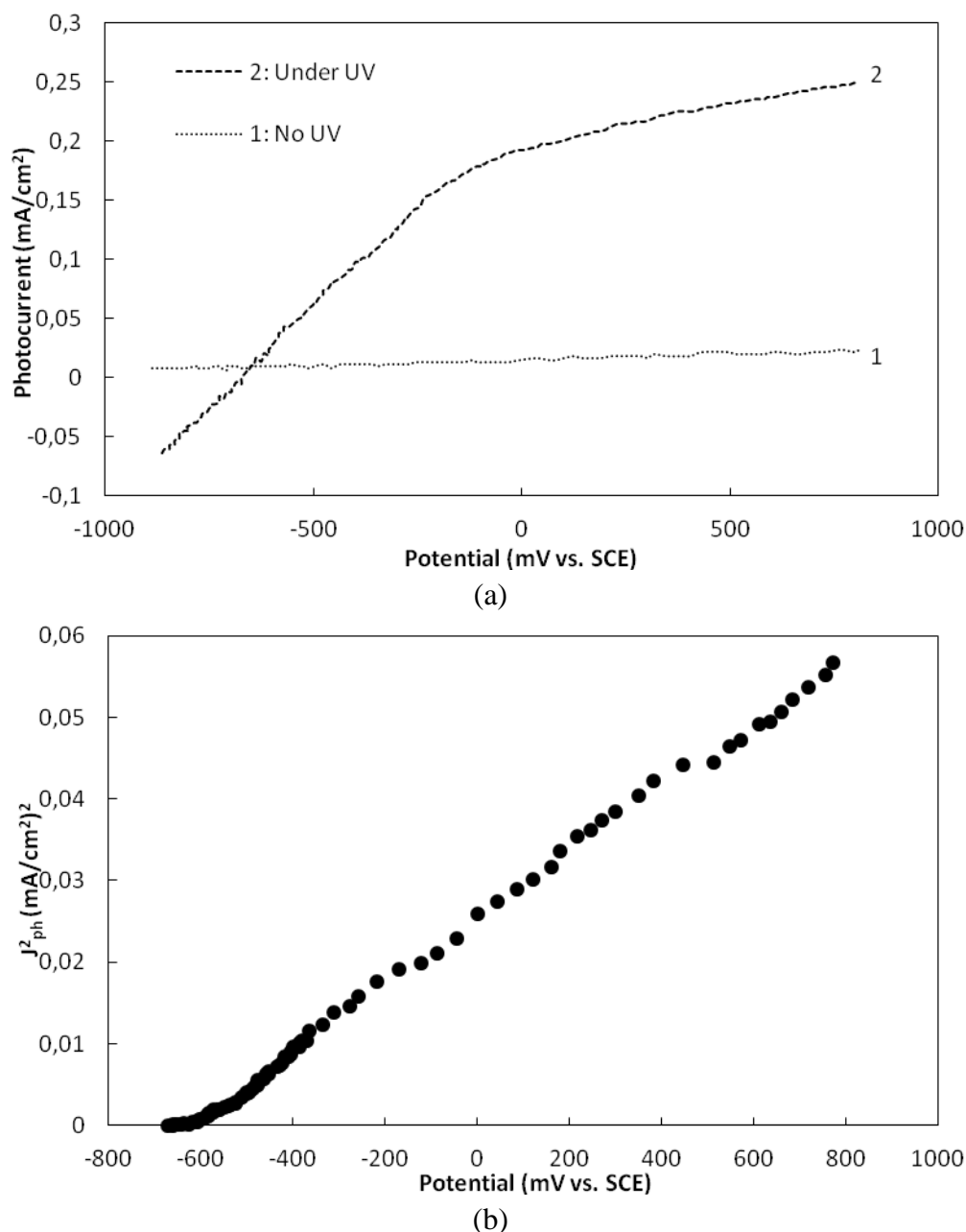


**Figure 9.** (a) Linear scan voltammograms obtained for the Ni- $TiO_2$ / $TiO_2$  multilayer coated electrodes heat treated at 450°C, in 0.1 M  $Na_2SO_4$  solution, without and under UV irradiation. Scan rate=10 mV/s and (b) the square wave of the photocurrent vs. applied potential under UV.



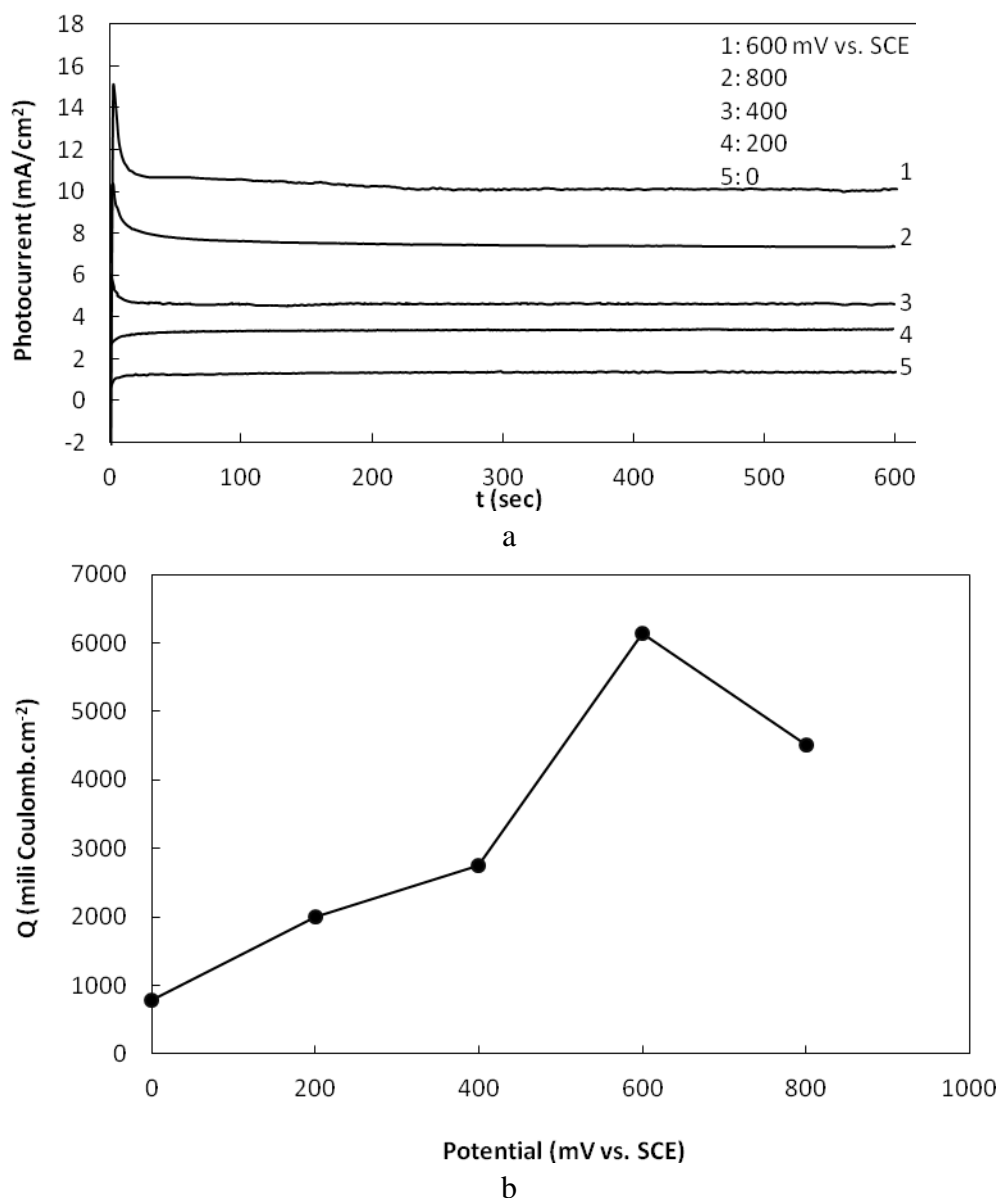
This value is negative enough to facilitate the electron transfer to hydrogen ions and promote the hydrogen evolution; thus, the dissociation of electron-hole pairs under the UV illumination is favored. [36]. To further calculate, the  $E_{fb}$  for the studied sample is -0.431 V vs. normal hydrogen electrode (NHE). Thereby,  $E_{cb}$  of  $TiO_2$  nanoparticles is about -0.431 V. The valence band potential ( $E_{vb}$ ) of the  $TiO_2$ -containing multilayer is approximated by the following equation:

$$E_g = E_{vb} - E_{cb} \quad (2)$$

$TiO_2$  nanoparticles in the anatase phase possess a band gap value of 3.2 eV; thus, the  $E_{vb}$  for the  $TiO_2$ -containing multilayer is approximated to be 2.76 V.

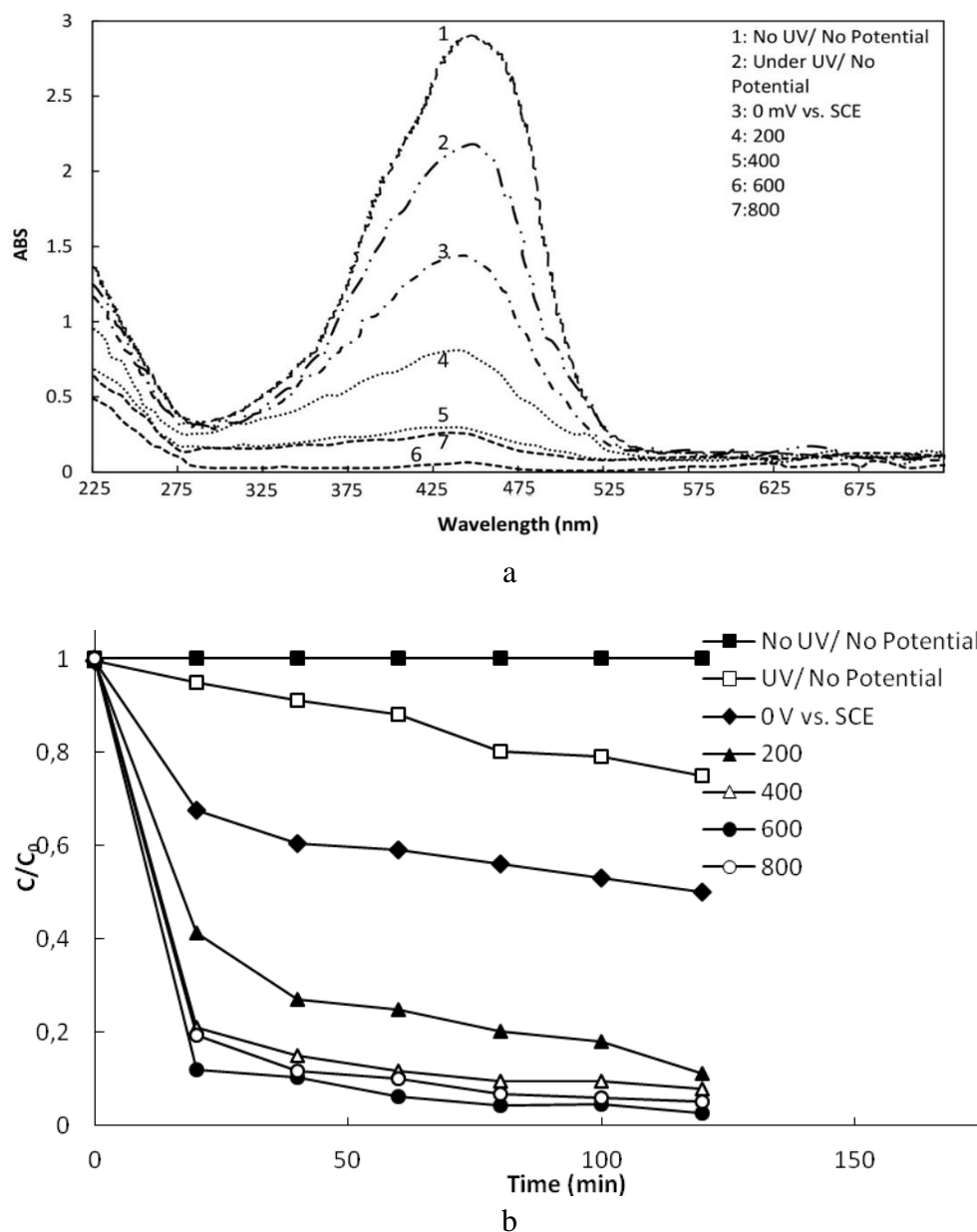
To improve the degradation rate of phenol by the Ni- $TiO_2$ / $TiO_2$  multilayer heat treated at 450°C, we applied five different potentials including 0, 200, 400, 600, and 800 mV vs. SCE along with 5h of UV irradiation in a mixture of 0.1 mol/L  $Na_2SO_4$  and 100 mg/L phenol. The PEC behavior of the multilayer is influenced by the applied voltage that promotes the migration of photoinduced electrons and inhibits the electron-hole recombination. Thus, the external voltage plays a crucial role in the PEC decomposition of contaminants. The initial 10 minutes of the photocurrent-time response of the samples are presented in Fig. 10 (a), and it can be observed that the i-t curves depend upon the applied potential, and as the external potential is increased in the range of 0 to 600 mV, the photocurrent density rises from 1.3 to 10.5 mA/cm<sup>2</sup>. However, when the applied potential is increased up to 800 mV, the photocurrent density decreases to 7.6 mA/cm<sup>2</sup>. This reduction is due to the fact that at 600 mV, the holes and electrons completely separate under UV illumination, and by the application of more positive potentials the by-reactions such as oxygen evolution would occur on the anode which leads to a reduction of the photocurrent produced by the  $TiO_2$ -containing coating [37]. The photoinduced current is representative of the PEC effectiveness, and the higher flow of UV-activated charges inside the multilayer increases the photocurrent magnitude [38]. Therefore, the multilayer under the applied potential of 600 mV exhibits the highest photocurrent density, and can successfully enhance the PEC efficiency.

Fig. 10 (b) represents the charge produced by the Ni- $TiO_2$ / $TiO_2$  multilayer heat treated at 450°C for phenol degradation versus the external potential applied in the PEC process. The photogenerated charge (coulomb) is measured by integrating i-t curves in Fig. 10 (a), and it can be observed that in the absence of an external voltage, the detected photocurrent for PC degradation test is estimated to be 791 mili-coulomb/cm<sup>2</sup>, while under the applied potential of 600 mV the quantity of the charge generated by the coating is approximately 8 times larger and is estimated to be 6149 mili-coulomb/cm<sup>2</sup>. This quantity indicates the higher amount of charge involved in the oxidation process as well as the higher PEC activity of the photoelectrode due to the higher amounts of the photogenerated electrons by the multilayer. However, as the applied potential exceeds the optimum value of 600 mV, the photogenerated charge amount decreases.



**Figure 10.** Effects of the applied potential on the (a) photocurrent-time profiles and (b) photogenerated charge obtained from Ni-TiO<sub>2</sub>/TiO<sub>2</sub> multilayer heat treated at 450 °C in a mixture of 0.1 mol/L Na<sub>2</sub>SO<sub>4</sub> and 100 mg/L phenol, under UV illumination.

The PEC performance of the Ni-TiO<sub>2</sub>/TiO<sub>2</sub> multilayer heat treated at 450 °C was also investigated by monitoring the degradation rate of phenol. The UV-Vis spectra obtained under no UV with no external potential, after 120 min of UV irradiation with no external potential, and after 120 min of UV along with 2h of applying five various potentials between zero and 800 mV on the anode coated with the TiO<sub>2</sub>-containing multilayer in a mixture consisting of Na<sub>2</sub>SO<sub>4</sub> and phenol are shown in Fig. 11 (a). The original phenol solution exhibits an intense peak at the wavelength of 450 nm and the intensity of this peak drastically reduces during the PEC treatment. In other words, the absorbance decreases under UV illumination with the increase of the applied potential up to 600 mV. However, when the applied potential exceeds 600 mV, the evolution of oxygen inhibits phenol decomposition and thus, the transmittance of the solution decreases and the absorbance increases.



**Figure 11.** (a) UV-vis spectra for the phenol using Ni-TiO<sub>2</sub>/TiO<sub>2</sub> multilayer heat treated at 450 °C as a photoelectrocatalyst and (b) effects of the applied potential on the photodegradation of phenol versus UV illumination duration.

According to Fig. 11 (b), when no potential is applied and the sample is not exposed to UV irradiation, the multilayer is not capable of degrading the phenol and the concentration of phenol remains constant. However, the UV illumination enhances the degradation efficiency, and after 120 minutes of UV irradiation, even in the absence of an external potential, the multilayer exhibits PC behavior and 25.01% of phenol is decomposed. When positive potentials are applied across the multilayer-coated photoelectrode along with the illumination of the UV light, the amount of the degraded phenol increases from 48.13% to 97.22% with the increase of the potential from zero to 600 mV, which can be ascribed to the reduced interaction of electrons and holes. When a positive external voltage is applied to the electrode coated with a TiO<sub>2</sub>-containing multilayer, the resultant voltage gradient within the multilayer provokes the UV-activated electrons and holes to flow in reverse

directions. Subsequently, the holes strongly oxidize surface-adsorbed water molecules to hydroxyl radicals. Moreover, the transference of photoactivated electrons is induced by the external electric field and the interactions between electrons and holes are inhibited [39]. Therefore, the amount of the decomposed phenol increases at more positive external potentials. However, the further increase in the applied potential beyond 600 mV does not enhance the phenol degradation, and as depicted in Fig. 11 (b), when the potential of 800 mV is applied on the anode, the amount of the degraded phenol is 95.01%. This can be attributed to the elimination of photoactivated charge carriers under the influence of the electric field or through a chemical reaction between electrons and the dissolved  $O_2$ . Moreover, at higher positive potentials, the volume of the oxygen evolved at the cathode increases and subsequently, the oxygen gas react with hydroxyl groups in the solution. Thus, the reduction in the amount of hydroxyl groups which account for the decomposition of phenol decreases the PEC efficiency of the  $TiO_2$ -containing multilayer [40].

In conclusion, it is evident that the PEC process is more efficient to degrade phenol, in which the almost complete removal of phenol (97.22%) is observed after 2h of UV illumination under 600 mV, while only 25.01% of phenol was removed in the PC process with the same illumination time.

#### 4. CONCLUSIONS

Ni- $TiO_2$ / $TiO_2$  multilayer coatings fabricated by the sol-modified PP electrodeposition were heated at different temperatures (100 to 550°C) for 3 h. The XRD data exhibited the existence of anatase  $TiO_2$  in nanostructured multilayers after being heated in the range of 200 to 450°C, while the transformation of the anatase to rutile occurred at temperatures higher than 450°C. Morphological studies conducted by AFM revealed that the enhanced surface roughness of multilayers was favored at higher heat treatment temperatures due to the removal of the remained carbon produced in the sol-gel process. Based on the XPS results, the concentration of surface hydroxyls was maximum for the film heat treated at 450°C after 1h of UV illumination, due to the presence of a greater amount of the hydrophilic anatase phase in this coating, leading to a favorable decrease in water contact angle down to 7.23°. The optimum PC activity was also observed for the multilayer heated at 450°C, for which a 53.64% MO degradation after 5h of UV illumination was achieved. The flat band potential that has a significant impact on the migration of electrons during the PEC reactions and the recombination of charge carriers was estimated to be -672 mV vs. SCE for this multilayer. Accordingly, this multilayer possessed the optimum PEC efficiency at the applied potential of 600 mV in comparison to other external potentials in similar test conditions. Furthermore, it was capable of decomposing 97.22% of phenol under the anodic potential of 600 mV along with 2h of simultaneous UV illumination.

#### ACKNOWLEDGEMENTS

This research was financially sponsored by the Department of Materials Science and Engineering at Sharif University of Technology.

## References

1. S.S. Bhogal, V. Kumar, S.S. Dhama and B.S. Pabla, *J. Electrochem. Sci. Eng.*, 5 (2015) 37.
2. W. Chen, Y. He and W. Gao, *Surf. Coat. Technol.*, 204 (2010) 2487.
3. Y.X. Wang, Y. Ju, S.J. Wang, W. Lu, B. Yan and W. Gao, *Mater. Res. Innov.*, 18 (2014) 1107.
4. M. Miyake, A. Takahashi and T. Hirato, *Int. J. Electrochem. Sci.*, 12 (2017) 2344.
5. X.B. Zheng and C.X. Ding, *J. Therm. Spray Technol.*, 9 (2000) 520.
6. I. Oja, A. Mere, M. Krunk, R. Nisumaa, C.H. Solterbeck and M.E.S. Souni, *Thin Solid Films*, 515 (2006) 674.
7. N. Chaisubanan, K. Pruksathorn, H. Vergnes, F. Senocq and M. Hunsom, *Int. J. Electrochem. Sci.*, 11 (2016) 1012.
8. T.T. Chu, Y.J. Hsiao and L.W. Ji, *Int. J. Electrochem. Sci.*, 10 (2015) 8951.
9. H.R. Bakhsheshi-Rad, E. Hamzah, M. Daroonparvar, M. Kasiri-Asgarani and M. Medraj, *Ceram. Int.*, 40 (2014) 14009.
10. J. Bautista-Ruiz, W. Aperador, A. Delgado and M. Diaz-Lagos, *Int. J. Electrochem. Sci.*, 9 (2014) 4144.
11. Y. Wang, W. Chen, A. Shakoor, R. Kahraman, W. Lu, B. Yan and W. Gao, *Int. J. Electrochem. Sci.*, 9 (2014) 4384.
12. Y. Wang, Y. Ju, S. Wei and B. Yan, *J. Electrochem. Soc.*, 161 (2014) 775.
13. B. Ranjith and G. Paruthimal Kalaigan, *Appl. Surf. Sci.*, 257 (2010) 42.
14. S. Mohajeri, A. Dolati and M. Ghorbani, *Surf. Coat. Technol.*, 262 (2015) 173.
15. J. Liqiang, S. Xiaojun, C. Weimin, X. Zili, D. Yaoguo and F. Honggang, *J. Phys. Chem. Solids*, 64 (2003) 615.
16. J. Jiang, G. Oberdorster, A. Elder, R. Gelein, P. Mercer and P. Biswas, *Nanotoxicology*, 2 (2008) 33.
17. B. Liu, X. Zhao, Q. Zhao, X. He and J. Feng, *J. Electron Spectrosc. Relat. Phenom.*, 148 (2005) 158.
18. Y. Zheng, C. Mo, F. Wang and Q. Mo, *Int. J. Electrochem. Sci.*, 10 (2015) 10344.
19. O. Ola and M.M. Maroto-Valer, *J. Photochem. Photobiol. C*, 24 (2015) 16.
20. H. Zhou, J. Ge, M. Zhang and S. Yuan, *Res. Chem. Intermed.*, 42 (2016) 1929.
21. X. Liu, R. Cong, L. Cao, S. Liu and H. Cui, *New J. Chem.*, 38 (2014) 2362.
22. D. Mahanta, U. Manna, G. Madras and S. Patil, *ACS Appl. Mater. Interfaces*, 3 (2011) 84.
23. S. Mohajeri, A. Dolati and M. Ghorbani, *JUFGNSM*, 49 (2016) 51.
24. C. Byrne, R. Fagan, S. Hinder, D.E. McCormack and S.C. Pillai, *RSC Adv.*, 6 (2016) 95232.
25. M.E. Simonsen, Z. Li and E.G. Sogaard, *Appl. Surf. Sci.*, 255 (2009) 8054.
26. S.D. Sharma, D. Singh, K.K. Saini, C. Kant, V. Sharma, S.C. Jain and C.P. Sharma, *Appl. Catal. A*, 314 (2006) 40.
27. L.B. Xiong, J.L. Li, B. Yang and Y. Yu, *J. Nanomater.*, 2012 (2012) 1.
28. C.E.B. Marino, P.A.P. Nascente, S.R. Biaggio, R.C. Rocha-Filho and N. Bocchi, *Thin Solid Films*, 468 (2004) 109.
29. R.N. Wenzel, *Ind. Eng. Chem.*, 28 (1936) 988.
30. Y.C. Wu, Z.M. Zhang, X.M. Huang, C.L. Shan and Z.P. Lin, *Adv. Mater. Res.*, 75 (2009) 13.
31. K. Rajeshwar, N.R. de Tacconi and C.R. Chenthamarakshan, *Chem. Mater.*, 13 (2001) 2765.
32. R. Daghrir, P. Drogui and D. Robert, *Ind. Eng. Chem. Res.*, 52 (2013) 3581.
33. X. Zheng, D. Li, X. Li, L. Yu, P. Wang, X. Zhang, J. Fang, Y. Shao and Y. Zheng, *Phys. Chem. Chem. Phys.*, 16 (2014) 15299.
34. M.A. Butler, *J. Appl. Phys.*, 48 (1977) 1914.
35. K. Kalyanansundaram and M. Gratzel, *Coord. Chem. Rev.*, 77 (1998) 347.
36. K. Rajeshwar, *J. Appl. Electrochem.*, 37 (2007) 765.
37. M. Ulmann and J. Augustynski, *Chem. Phys. Lett.*, 141 (1987) 154.

38. D. Jiang, H. Zhao, S. Zhang and R. John, *J. Phys. Chem. B*, 107 (2003) 12774.
39. M.D. Ward and A.J. Bard, *J. Phys. Chem.*, 86 (1982) 3599.
40. T. An, W. Zhang, X. Xiao, G. Sheng, J. Fu and X. Zhu, *J. Photochem. Photobiol. A: Chem.*, 161 (2004) 233.

© 2017 The Authors. Published by ESG ([www.electrochemsci.org](http://www.electrochemsci.org)). This article is an open access article distributed under the terms and conditions of the Creative Commons Attribution license (<http://creativecommons.org/licenses/by/4.0/>).